*Original Article*

# Stresses at the Cranial Base Induced by Rapid Maxillary Expansion

**Christof Holberg[a]; Ingrid Rudzki-Janson[b]**

**ABSTRACT**

**Objective:** An analysis of the distribution of stresses at the juvenile and adult cranial base after implementation of a rapid palatal suture expansion was the goal of this study. Of particular interest were stresses occurring near the cranial foramina containing vulnerable structures.

**Materials and Methods:** The stresses were simulated and analyzed using a finite elements model of the human cranial base. The model consisted of several skull bones (sphenoid, frontal bone, occipital bone, and the two temporal bones) with a total of 41,556 finite elements. To illustrate the differences between reactions in the juvenile and the adult, the differing bone elasticity was depicted as variations in the modulus of elasticity.

**Results:** At the juvenile cranial base only moderate stresses occurred during rapid palatal suture expansion, apparently precluding the likelihood of any serious complications in the area of the foramina. The situation in the adult, however, was different. Because of the reduced elasticity of the bony structures, considerable stress already occurred on light bending of the pterygoid process, especially in the area of the round foramen, the oval foramen, and the superior orbital fissure, all of which might lead to microfractures with injury of nervous and vascular structures.

**Conclusions:** The lower the bone elasticity on carrying out a rapid palatal suture expansion, the more important safety measures are for protecting the cranial base. For this reason the pterygomaxillary connection should be severed on both sides in adults when carrying out a surgically assisted palatal suture expansion. (*Angle Orthod* 2006;76:543–550.)

**KEY WORDS:** Cranial base; Skull base; Finite Elements Method; Rapid maxillary expansion



## INTRODUCTION

To separate the maxillary halves at the median palatine suture, relatively high forces are applied during a rapid palatal suture expansion. These forces act on the facial skull bones via anchoring teeth.[1] According to Isaacson et al[2] and Isaacson and Ingram,[3] cumulative forces of 100 N or more can be achieved on repeated activation of the central expansion screw that can lead to stress in the maxilla and the neighboring skull bone.[4,5] As Gardner and Kronman[6] demonstrated in rhesus monkeys, more removed anatomical structures are also affected by the stress, such as the cranial base. In one experimental animal, the rapid palatal suture expansion even led to an opening of more than one mm in the sphenooccipital synchondrosis.[6]

On clinical application of rapid palatal suture expansion in humans, serious complications leading to the assumption of an involvement of the cranial base are only rarely observed. Lanigan and Mintz[7] reported an increasing paresis of the oculomotor nerve in one patient after carrying out a surgically assisted rapid palatal suture expansion. Subsequent computed tomography (CT) revealed a cranial base fracture in the area of the sphenoid.[7]

But how does a rapid palatal suture expansion lead to induction of stress at the cranial base? Chaconas and Caputo[8] stated already in 1982 that rapid palatal suture expansion represents a problematic area at the pterygomaxillary connection because the sphenoid with its pterygoid process as an unmatched skull bone cannot participate in the transverse widening of the maxilla. As such, a lateral bending of the pterygoid process[4,8] occurs (see Figures 1 and 2) as well as a

[a] Resident, Department of Orthodontics, University of Munich, Munich, Bavaria, Germany.

[b] Professor and Department Chair, Department of Orthodontics, University of Munich, Munich, Bavaria, Germany.

Corresponding author: Dr. Christof Holberg, Department of Orthodontics, University of Munich, Goethestrasse 70, Munich, Bavaria 80336, Germany
(e-mail: christof.holberg@med.uni-muenchen.de)

Accepted: September 2005. Submitted: July 2005.

**FIGURE 1.** During rapid palatal suture expansion the two maxillary halves are moved apart in a transverse direction so that a lateral bending of the pterygoid process occurs (schematic representation of a native skull).

hindrance of the suture opening in the posterior region of the hard palate because of the increased resistance.[9–13] According to Melsen and Melsen,[14] one cannot count on a spontaneous opening of the pterygomaxillary connection during a rapid palatal suture expansion because of the extensive interlocking of the corresponding bone surfaces. According to studies by Jafari et al[4] the pterygoid process of the sphenoid is laterally bent by more than 2 mm during a rapid palatal suture expansion.

The goal of this study was therefore to examine the effects of this bending on the cranial base. The distribution pattern and the level of the stresses induced were to be analyzed for the cranial bases of juveniles and adults using a Finite Elements Method (FEM). Of particular interest was the stress distribution in the cranial base foramina with their vulnerable neural and vascular structures.

## MATERIALS AND METHODS

Numeric point cloud models of the individual skull bones consisting of a total of 365,785 individual points were constructed from the CT data. After reducing data redundancy and cross-linking of the point clouds

**FIGURE 2.** By bending the pterygoid process laterally, the induction of stresses, extensions, and deformations at the sphenoid body with its foramina occur (schematic representation of a plastic model produced by Somso, Coburg, Germany).

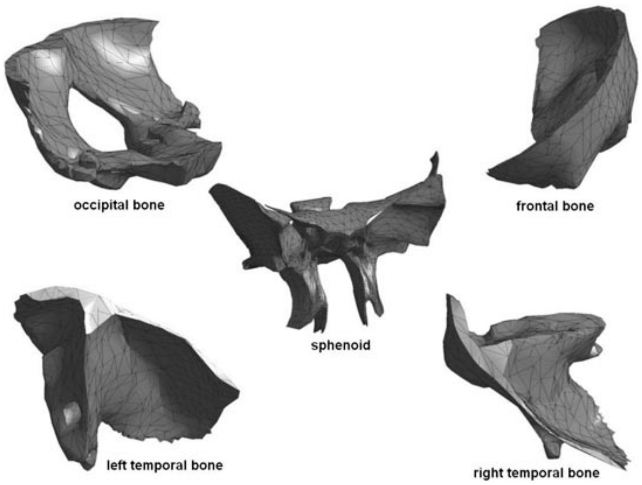


**FIGURE 3.** Individual partial model of the skull bones that were assembled into a complete simulation model of the cranial base considering the sutures.

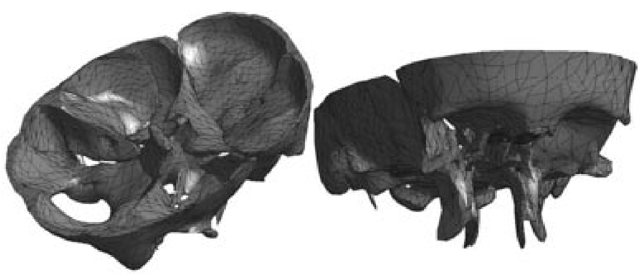

**FIGURE 4.** Resulting simulation model of the cranial base assembled from partial models of individual skull bones considering the individual sutures.

to polygonal meshes by Delauney triangulation, the individual Finite Elements Model was generated using a new, semiautomatic procedure.[15] These individual simulations of the frontal, occipital, sphenoid, and the two temporal bones (Figure 3) could now be assembled into an overall model of the cranial base that consisted of a total of 75,209 nodes and 41,556 tetrahedral elements (Figure 4).

Between the individual skull bones, an intimate sutural interlocking was now defined as a contact precondition. ANSYS WORKBENCH® from ANSYS Inc (Canonsburg, Penn) was used for all simulations. By referring to various literature sources,[4,5,16] a different modulus of elasticity was defined for the juvenile (8 GPa) and the adult cranial base (20 GPa). The Poisson ratio was determined as 0.3 for all simulations and a predefined fixed displacement of the nodes of the pterygoid process in the transverse direction was set as a storage condition. In all, 15 separate simulations could be carried out: five simulations for analyzing the stress distribution at the juvenile cranial base (bending of the pterygoid process of in each case 0.5, 1.0, 1.5, 2.0, and 2.5 mm), five simulations for analyzing the stress distribution at the adult cranial base (bending of the pterygoid process of in each case 0.5, 1.0, 1.5, 2.0, and 2.5 mm), and four simulations for analyzing the influence of bone elasticity (modulus of elasticity 5, 10, 15, and 20 GPa). All general experimental conditions for the simulations carried out are listed in Table 1.

On completion of the mathematical calculations, von Mises stresses (regional maxima) induced by bending of the pterygoid process could be measured using an interactive measurement tool in the vicinity of the var-

**Table 1.** General Experimental Conditions

| Parameter | Value |
|---|---|
| Number of parts | 5 |
| Number of nodes | 75,209 |
| Frontal bone | 18,499 |
| Sphenoid | 16,138 |
| Right temporal bone | 17,485 |
| Left temporal bone | 14,284 |
| Occipital bone | 8803 |
| Number of elements | 41,556 |
| Frontal bone | 9740 |
| Sphenoid | 8468 |
| Right temporal bone | 10,237 |
| Left temporal bone | 8280 |
| Occipital bone | 4831 |
| Sutural contact | Rigid |
| Young's modulus of juvenile sphenoid (GPa) | 8.0 |
| Young's modulus of adult sphenoid (GPa) | 20.0 |
| Elasticity of bone (GPa) | 5, 10, 15, 20 |
| Poisson's ratio of juvenile sphenoid | 0.3 |
| Poisson's ratio of adult sphenoid | 0.3 |
| Known transversal displacement | Nodes at the medial part of the pterygomaxillary junction |
| Magnitude of transversal displacement (mm) | 0.5, 1.0, 1.5, 2.0, and 2.5 |

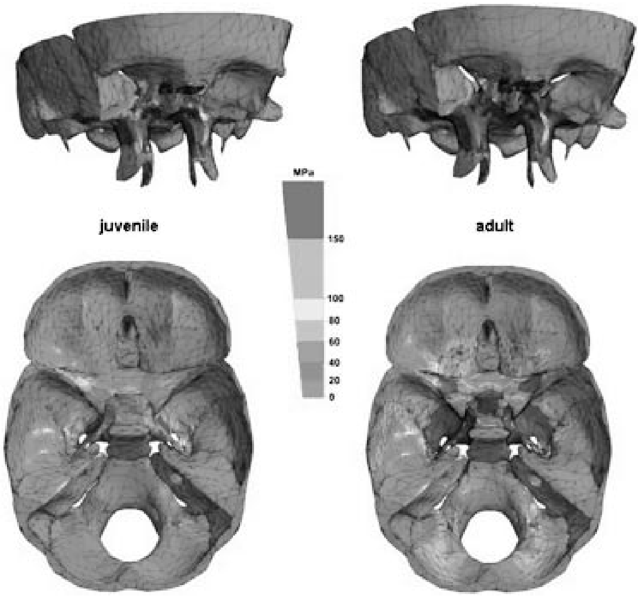


**FIGURE 5.** Stress distribution at the juvenile and adult cranial base on bending of the pterygoid process by 2.5 mm.

ious individual anatomical structures. A dynamic visualization of the stress buildup was also allowed by the software, as was the creation of virtual sections through the bony structures.

## RESULTS

The relative distribution pattern of the induced von Mises stresses showed a similar form and extent in all simulations and was quite clearly determined by the specific anatomical geometry of the cranial base (Figures 5 through 7). The differences between the juvenile and adult cranial base were reflected in the level of the induced stresses, whereas their relative distribution pattern was almost identical. The measured stresses of the juvenile cranial base were clearly lower than those of the adult cranial base (Figures 5 and 6). The further the pterygoid process was laterally bent, the higher were the stresses induced at the cranial base. All the individual anatomic measuring points affected by von Mises stresses are listed in Tables 2 to 4. On studying the influence of bone elasticity, a considerable increase in the stresses measured was seen on decreasing elasticity of the bony cranial base (Figure 7; Table 5).

### Sphenoid

In all simulations, the sphenoid presented the highest stresses of all the skull bones. The pterygoid process and the individual foramina were affected most strongly. At the carotid sulcus, the round foramen, the superior orbital fissure, the oval foramen, the lacerated foramen, the spinous foramen, and the optical fora-

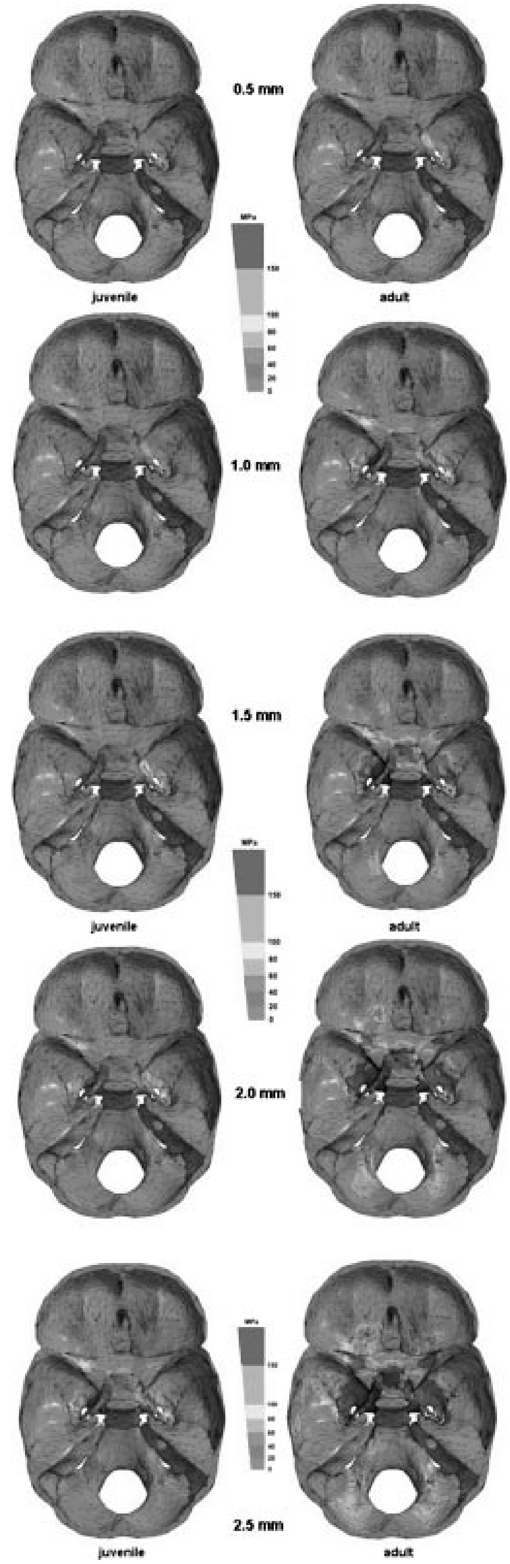


**FIGURE 6.** Stress distribution at the juvenile and adult cranial base on bending of the pterygoid process by 0.5 mm to 2.5 mm.

**Table 2.** Measured von Mises Stresses (in MPa) at the Anatomical Structures of the Cranial Base in the Juvenile and Adult After Bending of the Pterygoid Process by 2.5 mm

| Anatomical Structure | von Mises Stress (MPa) | |
|---|---|---|
| | Juvenile | Adult |
| Frontal crest | 9.2 | 18.6 |
| Orbital part of frontal bones | 22.8 | 34.4 |
| Greater wing of sphenoid | 15.3 | 41.8 |
| Lesser wing of sphenoid | 37.8 | 197.4 |
| Sphenoidal jugum | 36.2 | 92.4 |
| Pituitary fossa | 69.5 | 148.6 |
| Dorsum of sella | 4.7 | 5.4 |
| Carotid sulcus | 141.3 | 354.4 |
| Sphenooccipital synchondrosis | 21.2 | 38.8 |
| Medial lamina | 169.9 | 236.6 |
| Pterygoid fossa | 134.9 | 376.4 |
| Lateral lamina | 87.1 | 366.8 |
| Spinous foramen | 103.9 | 236.4 |
| Oval foramen | 137.8 | 344.2 |
| Lacerated foramen | 186.3 | 314.6 |
| Round foramen | 160.1 | 410.8 |
| Optic foramen | 61.3 | 210.2 |
| Superior orbital fissure | 181.6 | 426.8 |
| Internal auditory canal | 27.4 | 70.4 |
| Petrosal part of temporal bone | 28.1 | 70.2 |
| Squamosal part of temporal bone | 34.5 | 90.4 |
| Jugular foramen | 30.9 | 84.2 |
| Clivus | 36.2 | 124.6 |
| Occipital crest | 9.9 | 24.8 |
| Occipital condyle | 19.3 | 72.8 |

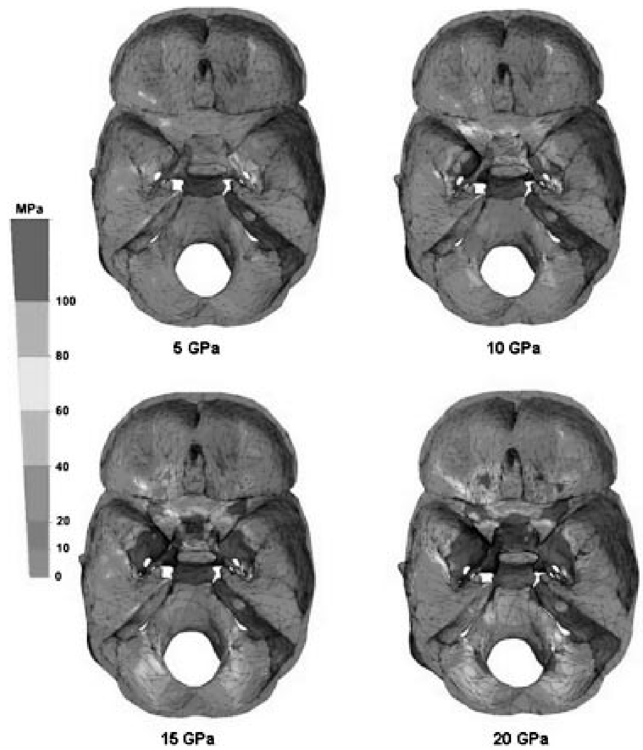


**FIGURE 7.** Dependence of stress development (von Mises stress) on bone elasticity of the cranial base, illustrated in the simulations as the modulus of elasticity.

**Table 3.** Measured von Mises Stresses at the Anatomical Structures of the Juvenile Cranial Base After Bending of the Pterygoid Process by 0.5 mm to 2.5 mm

| Anatomical Structure | von Mises Stress (MPa) | | | | |
|---|---|---|---|---|---|
| | 0.5 mm | 1.0 mm | 1.5 mm | 2.0 mm | 2.5 mm |
| Frontal crest | 3.5 | 4.7 | 7.6 | 8.2 | 9.2 |
| Orbital part of frontal bones | 2.9 | 6.4 | 8.2 | 13.4 | 22.8 |
| Greater wing of sphenoid | 4.7 | 7.0 | 12.3 | 12.8 | 15.3 |
| Lesser wing of sphenoid | 21.0 | 22.2 | 26.3 | 29.8 | 37.8 |
| Sphenoidal jugum | 9.3 | 18.1 | 25.7 | 31.5 | 36.2 |
| Pituitary fossa | 11.1 | 20.4 | 32.1 | 49.6 | 69.5 |
| Dorsum of sella | 0.0 | 1.2 | 1.2 | 1.8 | 4.7 |
| Carotid sulcus | 30.4 | 72.4 | 95.8 | 136.7 | 141.3 |
| Sphenooccipital synchondrosis | 1.8 | 7.0 | 12.3 | 14.6 | 21.2 |
| Medial lamina | 31.0 | 42.0 | 49.1 | 77.1 | 169.9 |
| Pterygoid fossa | 54.9 | 117.4 | 118.6 | 123.8 | 134.9 |
| Lateral lamina | 22.2 | 34.5 | 73.0 | 78.3 | 87.1 |
| Spinous foramen | 16.4 | 33.3 | 51.4 | 66.6 | 103.9 |
| Oval foramen | 26.3 | 59.6 | 79.4 | 114.5 | 137.8 |
| Lacerated foramen | 26.9 | 45.6 | 66.0 | 101.0 | 186.3 |
| Round foramen | 38.5 | 59.6 | 72.4 | 126.7 | 160.1 |
| Optic foramen | 15.8 | 36.8 | 50.2 | 56.1 | 61.3 |
| Superior orbital fissure | 33.9 | 71.2 | 104.5 | 130.8 | 181.6 |
| Internal auditory canal | 4.1 | 9.9 | 15.8 | 21.0 | 27.4 |
| Petrosal part of temporal bone | 4.7 | 8.8 | 14.0 | 18.7 | 28.1 |
| Squamosal part of temporal bone | 6.4 | 9.3 | 19.9 | 21.0 | 34.5 |
| Jugular foramen | 5.8 | 19.9 | 22.2 | 25.7 | 30.9 |
| Clivus | 5.3 | 10.5 | 16.9 | 21.6 | 36.2 |
| Occipital crest | 1.2 | 2.9 | 4.7 | 5.3 | 9.9 |
| Occipital condyle | 2.3 | 3.5 | 6.4 | 9.3 | 19.3 |

**Table 4.** Measured von Mises Stresses at the Anatomical Structures of the Adult Cranial Base After Bending of the Pterygoid Process by 0.5 mm to 2.5 mm

| Anatomical Structure | von Mises Stress (MPa) | | | | |
|---|---|---|---|---|---|
| | 0.5 mm | 1.0 mm | 1.5 mm | 2.0 mm | 2.5 mm |
| Frontal crest | 5.0 | 5.4 | 11.8 | 16.8 | 18.6 |
| Orbital part of frontal bones | 8.4 | 16.2 | 24.8 | 32.6 | 34.4 |
| Greater wing of sphenoid | 14.2 | 27.2 | 33.0 | 36.4 | 41.8 |
| Lesser wing of sphenoid | 44.8 | 82.8 | 136.4 | 156.8 | 197.4 |
| Sphenoidal jugum | 17.4 | 33.4 | 48.2 | 57.4 | 92.4 |
| Pituitary fossa | 30.8 | 54.8 | 81.4 | 107.6 | 148.6 |
| Dorsum of sella | 0.8 | 1.8 | 2.8 | 3.6 | 5.4 |
| Carotid sulcus | 80.2 | 142.8 | 247.0 | 307.4 | 354.4 |
| Sphenooccipital synchondrosis | 7.0 | 16.2 | 20.6 | 27.4 | 38.8 |
| Medial lamina | 62.4 | 125.2 | 150.8 | 196.8 | 236.6 |
| Pterygoid fossa | 80.4 | 122.4 | 183.0 | 296.6 | 376.4 |
| Lateral lamina | 80.8 | 152.8 | 216.4 | 245.0 | 366.8 |
| Spinous foramen | 52.4 | 79.2 | 142.4 | 174.8 | 236.4 |
| Oval foramen | 64.8 | 137.4 | 218.2 | 285.8 | 344.2 |
| Lacerated foramen | 75.0 | 154.4 | 206.8 | 221.4 | 314.6 |
| Round foramen | 82.4 | 168.6 | 250.4 | 273.6 | 410.8 |
| Optic foramen | 30.4 | 50.6 | 113.6 | 209.4 | 210.2 |
| Superior orbital fissure | 86.4 | 171.4 | 271.8 | 356.6 | 426.8 |
| Internal auditory canal | 10.6 | 16.6 | 38.4 | 56.6 | 70.4 |
| Petrosal part of temporal bone | 8.4 | 24.2 | 31.8 | 37.2 | 70.2 |
| Squamosal part of temporal bone | 12.0 | 25.4 | 36.8 | 50.8 | 90.4 |
| Jugular foramen | 11.2 | 18.6 | 27.2 | 44.8 | 84.2 |
| Clivus | 14.2 | 29.0 | 41.4 | 57.8 | 124.6 |
| Occipital crest | 4.0 | 7.4 | 10.6 | 14.2 | 24.8 |
| Occipital condyle | 7.0 | 12.2 | 15.2 | 19.2 | 72.8 |

**Table 5.** Measured von Mises Stresses at the Anatomical Structures of the Cranial Base After Bending of the Pterygoid Process of 2.0 mm and Their Dependence on Bone Elasticity

| Anatomical Structure | von Mises Stress (MPa) | | | |
|---|---|---|---|---|
| | 5 GPa | 10 GPa | 15 GPa | 20 GPa |
| Frontal crest | 4.2 | 14.1 | 15.3 | 16.8 |
| Orbital part of frontal bones | 8.6 | 16.3 | 24.5 | 32.6 |
| Greater wing of sphenoid | 13.4 | 28.3 | 32.6 | 36.4 |
| Lesser wing of sphenoid | 46.7 | 90.1 | 128.3 | 156.8 |
| Sphenoidal jugum | 17.7 | 22.6 | 48.6 | 57.4 |
| Pituitary fossa | 22.9 | 54.2 | 78.3 | 107.6 |
| Dorsum of sella | 0.8 | 1.5 | 2.7 | 3.6 |
| Carotid sulcus | 79.9 | 166.1 | 238.9 | 307.4 |
| Sphenooccipital synchondrosis | 7.5 | 14.9 | 20.6 | 27.4 |
| Medial lamina | 62.5 | 135.4 | 148.5 | 196.8 |
| Pterygoid fossa | 77.5 | 156.9 | 193.8 | 296.6 |
| Lateral lamina | 73.3 | 165.3 | 200.4 | 245.0 |
| Spinous foramen | 55.4 | 83.8 | 144.2 | 174.8 |
| Oval foramen | 82.6 | 158.1 | 238.9 | 285.8 |
| Lacerated foramen | 53.4 | 112.4 | 176.6 | 221.4 |
| Round foramen | 76.4 | 135.9 | 198.5 | 273.6 |
| Optic foramen | 57.9 | 86.2 | 138.5 | 209.4 |
| Superior orbital fissure | 84.8 | 135.7 | 273.8 | 356.6 |
| Internal auditory canal | 10.9 | 20.5 | 34.8 | 56.6 |
| Petrosal part of temporal bone | 11.8 | 19.8 | 32.4 | 37.2 |
| Squamosal part of temporal bone | 12.2 | 24.1 | 39.7 | 50.8 |
| Jugular foramen | 9.3 | 21.7 | 26.5 | 44.8 |
| Clivus | 14.3 | 27.6 | 43.8 | 57.8 |
| Occipital crest | 3.6 | 5.2 | 12.3 | 14.2 |
| Occipital condyle | 3.9 | 6.5 | 12.1 | 19.2 |

men in particular, very high stresses were always found (see Figures 5 through 7). The values at the greater and lesser wing of the sphenoid, at the sphenoidal jugum, and at the pituitary fossa were usually lower but still higher than at most measurement points on the other skull bones. With a 2.5-mm lateral bending of the pterygoid process, the induced stresses at the foramina of the juvenile cranial base were between 61.3 and 186.3 MPa, whereas at the foramina of the adult cranial base they were between 210.2 and 426.8 MPa. With less bending of the pterygoid process, the stresses were correspondingly smaller (see Tables 3 and 4). With the experiments studying the influence of bone elasticity on the foramina of the sphenoid with a 2.0-mm bending and a modulus of elasticity of 15 GPa, stresses between 138.5 and 273.8 MPa were determined, whereas with a modulus of elasticity of five GPa, values between 53.4 and 84.8 MPa were apparent.

### Temporal bone

The measured stresses at all measurement points of the temporal bone were far lower than they were at the sphenoid. The measured values at the temporal bone in the simulations at the juvenile cranial base were always less than 50 MPa. The largest relative stresses occurred in the medial region of the petrous part and at the squamous bone. The lowest, on the other hand, were found in the lateral part of the petrous part (see Figures 5 through 7). Values measured in the internal auditory canal were moderate. All measured individual values at the temporal bone are listed in Tables 2 to 5. Even with a very low bone elasticity (Young's modulus = 20 GPa), the measured stresses with a lateral bending of the pterygoid process of 2.0 mm were between 37.2 and 50.8 MPa.

### Frontal bone

At the frontal bone as well, the stresses were far lower than they were at the sphenoid. With a lateral bending of the pterygoid process of 2.5 mm, the stress measured in adult bone in the area of the orbital part of the frontal bone was 34.4 MPa, whereas in the juvenile bone it was 22.8 MPa. At the frontal crest the values were even lower. Here, the von Mises stresses with a 2.5-mm bending of the pterygoid process were 18.6 MPa at the adult cranial base and 9.2 MPa at the juvenile cranial base. On studying the influence of bone elasticity when laterally bending the pterygoid process by 2.0 mm, stresses of 24.5 MPa in the orbital part of the frontal bone and 15.3 MPa at the frontal crest were seen (Young's modulus 15 GPa). Peak stresses achieving those seen at the measurement points in the sphenoid could not be observed at the frontal bone (see Figures 5 through 7). All individual values measured at the frontal bone are listed in Tables 2 to 5.

### Occipital bone

On bending the pterygoid process laterally by 2.5 mm, stresses at the clivus of 36.2 MPa, at the occipital crest of 9.9 MPa, and at the occipital condyles of 19.3 MPa were measured at the juvenile cranial base, whereas values with the adult cranial base were much higher at 124.6 MPa for the clivus, 24.8 MPa for the occipital crest, and 72.8 MPa for the occipital condyle. All stresses were on average greater than they were at the frontal bone but less than those at the sphenoid. For simulations with moderate bone elasticity (Young's modulus 15 GPa), the stresses lay between 12.1 and 43.8 MPa (see Table 5).

## DISCUSSION

The papers of Iseri et al[5] and Jafari et al[4] revealed the FEM to be a valuable tool for stress and deformation analysis with rapid palatal suture expansion. The precision of the virtual simulation depends on the accuracy of the Finite Element model, because the simulation approximates the real process.

An important criterion is the precision of geometric illustration by the simulation models. Iseri et al[5] in 1998 for his analyses on the palatal suture expansion used a Finite Elements Model of the complete skull with just 2349 individual shell elements, which geometrically depicted the actual anatomical conditions only very inaccurately.[5] The Finite Elements Model proposed by Jafari et al[4] in the year 2003 was already markedly more differentiated with 6951 single elements but could not yet define any detailed anatomical structures in the area of the cranial base. The simulation model used in this study that was assembled from several individual skull bones consisted of 41,556 individual tetrahedral-shaped elements and allowed for the first time a differentiated assessment of stress development at fine anatomical structures of the human cranial base. Nevertheless, this model also represents an extreme idealization of the actual conditions because inter- and intraindividual variations in bone thickness, quality, and bone elasticity are not considered. As such, a cautious and considered interpretation of the results is demanded and predictions or statements of only a relative nature should be made from the results.

When analyzing the results it becomes apparent that the absolute level of the induced stresses greatly depends on bone elasticity in the simulations. The more nonelastic the bony structures were, the higher were the stresses induced on the structures of the cranial base. All stresses at the juvenile cranial base lay in a moderate range, whereas at some structures of the adult cranial base, high individual values occurred that might explain the origin of microfractures that injure neural and vascular structures.

The cranial base fracture described by Lanigan and Mintz[7] in the area of the sphenoid is plausible because the fracture course depicted in the CT exactly follows areas in which persistently high stresses were measured in this study. Also, the opening of the sphenooccipital synchondrosis confirmed by Gardner and Kronman[6] can be considered consistent with the present results because stresses can be shown at the transition of the sphenoid to the occipital bone that can lead to dehiscence of a still unossified synchondrosis. With the simulations carried out in this study, the highest stresses were measured mostly at the superior orbital fissure, at the carotid sulcus, at the round foramen, at the oval foramen, at the lacerated foramen, and at the spinous foramen, ie, all apertures in the cranial base through which important nervous and vascular structures run. These apertures seem to be regions of increased vulnerability because of crossing neural and vascular structures. As a consequence of the present measurements, where a rapid palatal suture expansion is being carried out, more attention should be paid to the possibility of hyperthesia in the areas supplied by the individual brain nerves or to transient disorders in eye motility. Discrete, temporary neurologic disorders can reflect the presence of microfractures. An actual cranial base fracture, on the other hand—as observed by Lanigan and Mintz[7] in one adult patient—should be considered extremely rare.

In children and adolescents where bony elasticity is very high, the present results suggest that undesirable side effects should not be expected at all in the area of the cranial base after a rapid palatal suture expansion. The level of stresses induced at the cranial base was not only influenced by bone elasticity but also by the extent of lateral bending of the pterygoid process. As Krebs[11–13] already showed, the opening of the median palatine suture on palatal suture expansion does not usually run parallel and in the posterior area is only half as large on average as it is between the incisures. The cause for this, according to Chaconas and Caputo,[8] is the pterygomaxillary connection that binds the unmatched sphenoid with the two (to be) separated maxillary halves in the posterior area.

According to the calculations of Jafari et al,[4] lateral bending of the pterygoid process amounts to approximately 2 mm so that the bending of between 0.5 and 2.5 mm assumed in this study can be considered realistic. Only a fixed pterygomaxillary connection, where spontaneous opening is not to be expected during a rapid palatal suture expansion according to Melsen and Melsen,[14] allows the transmission of stress to the skull base. Measures for protecting the cranial base become all the more important the smaller the elasticity of the bone structures, particularly the pterygoid process. Surgical severance of the pterygomaxillary connection should wherever possible be carried out bilaterally as a protective measure for adult patients, as proposed by Matteini and Mommaerts.[17]

## CONCLUSIONS

- Rapid palatal suture expansion leads to moderate stresses at the cranial base in children and adolescents so that serious complications are unlikely in the area of the juvenile cranial base.
- During adulthood, lateral bending of the pterygoid process during a rapid palatal suture expansion leads to a marked development of stress, particularly in the area of the sphenoid.
- The superior orbital fissure, that oval foramen, the spinous foramen, the round foramen, the lacerated foramen, the optic foramen, and the carotid sulcus are particularly affected.
- The lower the patient's bone elasticity during a rapid palatal suture expansion, the more important are protective measures for protecting the cranial base.
- The pterygomaxillary connection should be completely severed on both sides in adults who are undergoing a surgically assisted palatal suture expansion.

## REFERENCES

1. Göz G. Rasche Gaumennahterweiterung. In: Diedrich P, ed. *Praxis der Zahnheilkunde.* Kieferorthopädie. Band II. München, Jena, Germany: Urban und Fischer; 2000:271–279.
2. Isaacson RJ, Wood JL, Ingram AH. Forces produced by rapid maxillary expansion. Part I. Design of the force measuring system. *Angle Orthod.* 1964;34:256–260.
3. Isaacson RJ, Ingram AH. Forces produced by rapid maxillary expansion. Part II. Forces present during treatment. *Angle Orthod.* 1964;34:261–270.
4. Jafari A, Shetty K, Kumar M. Study on stress distribution and displacement of various craniofacial structures following application of transverse orthopedic forces—a three-dimensional FEM study. *Angle Orthod.* 2003;73:12–20.
5. Iseri H, Tekkaya AE, Oztan O, Bilgic S. Biomechanical effect of rapid maxillary expansion on the craniofacial skeleton, studied by the finite element method. *Eur J Orthod.* 1998;20:347–356.
6. Gardner GE, Kronman JH. Cranioskeletal displacement caused by rapid palatal expansion in the Rhesus monkey. *Am J Orthod.* 1971;59:146–155.
7. Lanigan DT, Mintz SM. Complications of surgically assisted rapid palatal expansion: review of the literature and report of a case. *J Oral Maxillofac Surg.* 2002;60:104–110.
8. Chaconas SJ, Caputo AA. Observation of orthopedic force distribution produced by maxillary orthodontic appliances. *Am J Orthod.* 1982;82:492–501.
9. Inoue N. Radiographic observation of rapid expansion of human maxilla. *Bull Tokyo Med Dent Univ.* 1970;17:249–261.
10. Wertz RA. Skeletal and dental changes accompanying rapid midpalatal suture opening. *Am J Orthod.* 1970;58:41–66.
11. Krebs A. Expansion of the midpalatal suture studied by means of metallic implants. *Eur Orthod Soc Rep.* 1958;34:163–171.
12. Krebs A. Expansion of midpalatal suture studied by means of metallic implants. *Acta Odontol Scand.* 1959;17:491–501.
13. Krebs A. Rapid expansion of midpalatal suture by fixed appliances. An implant study over a 7 year period. *Rep Congr Eur Orthod Soc.* 1964;40:131–142.
14. Melsen B, Melsen F. The postnatal development of the palatomaxillary region. Studies on human autopsy material. *Am J Orthod.* 1982;82:329–342.
15. Holberg C. Method, Device and Computer Product for Making an 3D Finite Element Model. European Patent Office WIPO (PCT) 2003; Publication Number WO 03/10276.
16. Tanne K, Hiraga J, Kakiuchi K, Yamagata Y, Sakuda M. Biomechanical effect of anteriorly directed extraoral forces on the craniofacial complex: a study using the finite element method. *Am J Orthod Dentofac Orthop.* 1989;95:200–207.
17. Matteini C, Mommaerts MY. Posterior transpalatal distraction with pterygoid disjunction: short-term model study. *Am J Orthod Dentofac Orthop.* 2001;120:498–502.